High-Yield Cellulose Nanocrystals from Bleached Eucalyptus Fibers via Maleic Acid Hydrothermal Treatment and High-Pressure Homogenization

Amira Najahi, Marc Delgado-Aguilar, Jean-Luc Putaux, Sami Boufi

Biomacromolecules

Open Access

pubs.acs.org/Biomac

Article

High-Yield Cellulose Nanocrystals from Bleached Eucalyptus Fibers via Maleic Acid Hydrothermal Treatment and High-Pressure Homogenization

Amira Najahi, Marc Delgado-Aguilar, Jean-Luc Putaux, and Sami Boufi*

Cite This: *Biomacromolecules* 2025, 26, 1372−1385

Read Online

ACCESS | Metrics & More | Article Recommendations | Supporting Information

ABSTRACT: This study reports the preparation of cellulose nanocrystals (CNCs) from commercial bleached eucalyptus Kraft pulp (BEKP) using a hydrothermal treatment in the presence of maleic acid (MA), followed by high-pressure homogenization. Compared with conventional hydrolysis methods, this approach offers significant advantages, including lower acid concentration, higher yield, and milder processing conditions. CNCs were produced with a high yield (70−85 wt %) by high-pressure homogenization of hydrothermally treated BEKP fibers with 10−20 wt % maleic acid at 150 °C, giving rise to a stable translucent gel of CNCs with a rod-like morphology (200−400 nm length and 10−40 nm width). The reinforcing potential of the CNCs was also assessed by preparing nanocomposite films with CNC contents of up to 15 wt %, and the results were compared to commercial CNCs from CelluForce. Additionally, their biodegradability in aquatic media was assessed using biological oxygen demand, with results compared to those of neat cellulose fibers. The MA-assisted hydrothermal process is an environmentally friendly alternative to conventional CNC production methods, offering higher yields and enhanced thermal stability while preserving a strong reinforcing property.

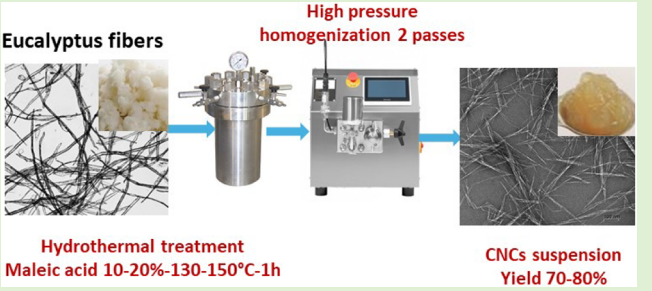

1. INTRODUCTION

Owing to their singular properties, including outstanding stiffness with a modulus exceeding 100 GPa, nanoscale needle-like morphology, low density (1.6 g cm^{-3}), high specific surface area, and environmental sustainability, cellulose nanocrystals (CNCs) have gained significant interest from both academia and industry. They are promising for various applications in a myriad of fields, including innovative materials,[1] nanocomposite reinforcement, strength additives for paper, thin films, electronics and sensors,[2] emulsifying and stabilizing agents for surfactant-free emulsions,[3] biomedical devices,[4] and rheology modifiers, to name a few of them.

Despite extensive research in the field of CNCs, challenges remain in their production and processing, particularly when H_2SO_4 is used to hydrolyze cellulose fibers. While H_2SO_4 is highly effective at achieving hydrolysis in a relatively short time (around 1 h at 40−50 °C), its corrosive and hazardous nature generates several drawbacks, including environmental concerns, severe equipment corrosion, safety considerations, difficulties in liquid acid recovery, and relatively moderate yield in CNCs (ca. 20−30 wt %) due to the excessive degradation of cellulose. Indeed, in most studies, the yield in CNCs using H_2SO_4 or HCl typically ranges between 10 and 60 wt %, depending on parameters such as the hydrolysis temperature andtime, and the chemical composition of the fibers. All of these concerns hamper the widespread industrial production of CNCs and induce additional operational costs.

Moreover, H_2SO_4 hydrolysis alters the properties of the resulting CNCs, mainly due to the formation of sulfate half-ester groups on their surface. While these groups enhance colloidal stability through electrostatic repulsion, their presence reduces the thermal stability of CNCs, causing premature degradation over 200 °C. This limits the use of CNCs as reinforcing nanofillers in polymer matrices, especially via melt-processing methods.[5]

An alternative method using HCl instead of H_2SO_4 has also been explored, yielding CNCs with better thermal properties and higher yields. Yields exceeding 80%—and even up to 93%—have been reported when using HCl under hydrothermal conditions, which helps shorten the hydrolysis time. These high yields were obtained using highly pure cellulose sources, such as cotton or microcrystalline cellulose.[6] However, HCl has notable drawbacks, including equipment corrosion, typically low yields (around 20 wt %), and flocculation of the

Received: December 11, 2024
Revised: January 17, 2025
Accepted: January 21, 2025
Published: January 30, 2025

resulting aqueous suspensions, primarily due to a lack of colloidal stability.[7]

To address some of the drawbacks associated with HCl or H_2SO_4 hydrolysis and facilitate the production of CNCs, the development of alternative environmentally friendly production processes is imperative, using milder and safer conditions as well as alternative acids. These methods aim at reducing the environmental impact of the hydrolysis process, improving control over CNC properties, and enhancing the overall sustainability. In this sense, the use of recyclable organic acids appears to be a promising and sustainable strategy that has attracted increasing interest due to the possibility of operating under milder reaction conditions, preventing equipment corrosion, and allowing to recover the organic acid after the process. A recent review reported on the most recent advances in the sustainable preparation of CNCs via solid acid hydrolysis.[8]

Oxalic, citric, and maleic acids (OA, CA, and MA, respectively) are the most studied organic acids for the preparation of CNCs via the acid hydrolysis of bleached cellulose fibers. In 2016, Chen et al.[9] successfully produced nanocellulose composed of CNCs and cellulose nanofibrils (CNFs) from bleached eucalyptus kraft pulp (BEKP) with high thermal stability by using organic acid hydrolysis (OA or MA) at a concentration between 50 and 70 wt %, a temperature ranging from 90 to 120 °C, and operating at ambient pressure. A yield in CNCs of around 60 wt % was achieved via ball milling-assisted OA hydrolysis at 80 °C for 4 h.[10] CA has also been proposed for CNC production, resulting in nanomaterials with good colloidal and thermal stability. Bondancia et al. prepared CNCs using CA hydrolysis at 120 °C for 3 to 6 h. However, the yield was 23 wt %, and CNCs were recovered by intensive centrifugation to separate them from the microsized fraction.[11]

MA has also been used to hydrolyze bleached cellulose fibers and produce nanocellulose. For instance, carboxylated CNCs and CNFs were prepared from bleached pulp fibers via MA hydrolysis.[12] The CNCs were recovered by centrifugation, and the residual fibers were homogenized using a microfluidizer to disintegrate them into CNFs. However, a concentration of MA over 50 wt % was necessary to ensure a high yield in nanocellulose. In addition, the fraction in CNC did not exceed 5 wt %, and most of the nanocellulose was in the form of CNFs. A similar approach was adopted for the production of lignin-containing CNCs and CNFs (LCNCs and LCNFs, respectively) using two unbleached mixed hardwood chemical pulps at 120 °C for 2 h with a 60 wt % MA solution and a pulp-to-acid weight ratio of 1:10.[13] However, the yield in LCNCs was below 6 wt %, highlighting the low efficiency of the process. A ball-milling pretreatment combined with MA hydrolysis in a 60 wt % MA solution at 120 °C for 2 h contributed to increasing the yield, ranging between 11 and 24 wt %.[14] In that work, the authors claimed that ball milling broke down and opened the structure of cellulosic fibers, thus exposing more hydroxyl groups at the surface and promoting the access of acid molecules to the fibers.

In most works dealing with the production of CNCs via organic acid hydrolysis, the acid concentration was typically quite high, often exceeding 50 wt %, which contributed to high production costs and challenges in acid recovery. In addition, for most of the reported works, the yield in CNCs was relatively low (<30 wt %), and CNCs were often mixed with microsized residual fibers, making the separation of CNCs by centrifugation necessary.

For all these reasons, the objective of the present work was to produce high-yield CNCs (>50 wt %) by MA hydrolysis at low concentration combined with high-pressure homogenization (HPH). The MA hydrolysis was performed under hydrothermal conditions at temperatures between 135 and 150 °C, reducing the MA concentration below 20 wt %, and yielding CNCs after HPH disintegration. This study presents an eco-friendly and efficient method for producing CNCs from bleached pulp, achieving yields exceeding 50 wt % while maintaining high thermal stability. The CNCs were thoroughly characterized using various techniques, and their properties were compared to those produced by conventional acid hydrolysis methods.

2. EXPERIMENTAL SECTION

2.1. Materials. The BEKP was kindly provided by Torraspapel (Spain). All of the chemicals used in this investigation, including maleic acid (MA), were purchased from Sigma-Aldrich (Spain) and were used as received without additional purification. Commercial-grade CNCs (CF-CNCs, from CelluForce, Canada) were used as a reference.

2.2. Morphology. The morphology of the pulp fibers, namely, the fiber length, width, fine content, and coarseness, was characterized by image analysis of a diluted suspension flowing in a transparent flat chamber and observed with a CCD video camera. More than 30,000 fibers were measured using a Morfi LB-01 analyzer (Techpap, France). The length threshold for fine determination was set to 200 μm. The initial fibers and hydrothermally treated samples were observed with a Zeiss Axiophot II optical microscope equipped with an Olympus SC50 digital camera. Homogenized gels were observed under polarized light and under differential interference contrast.

2.3. CNC Preparation. The BEKP fibers were first dispersed in water using a high-speed disintegrator equipped with propeller blades at a speed of 10^4 rpm for 10 min until complete homogeneous dispersion of the fibers at about 5 wt %. Then, the fiber suspension was subjected to a hydrothermal treatment in the presence of different concentrations of MA, at a temperature ranging from 135 to 150 °C, for 2 and 3 h. The pressure inside the reactor ranged from 300 to 500 kPa, depending on the temperature (p = 300 kPa at 135 °C and 500 kPa at T = 150 °C). The pH of the suspension before treatment ranged between 2.5 and 3, depending on the MA concentration.

The hydrothermal treatment was carried out in a jacketed, pressurized 3-L stainless steel reactor equipped with stirring. In a typical experiment, 300 g of the fibers (in the form of a suspension) were added to the MA solution so that the solid-to-liquid ratio was kept at 1:10. Then, the temperature was raised (135 or 150 °C), and the suspension was kept under mechanical stirring for 2 or 3 h, depending on the selected conditions. After this treatment, the suspension was recovered by filtration through a 10 μm polyamide screen fabric and thoroughly washed with water until achieving a nearly similar pH as the water used for the washing treatment. The different samples will be referred to as t-M-T in the following, where t, M, and T stand for time (in h), MA concentration (in wt %), and temperature (in °C), respectively. The treated fibers were then dispersed in water until achieving a consistency of 2 wt % and passed through a high-pressure homogenizer (PANDA Plus 2000, GEA Niro Soavi, Italy). The homogenization sequence was set at 2 passes at 300 bar, followed by 2 passes at 600 bar. The overall CNC production process is illustrated in Scheme 1.

2.4. Carboxyl Content. The carboxyl content (CC) was determined by conductometric titration on the fibers before performing the HPE, following the method described elsewhere.[15] In brief, about 100 mg of fibers were suspended in 15 mL of a 0.01 N HCl solution to protonate the carboxyl groups. The suspension was then back-titrated by adding a 0.01 N NaOH solution while continuously measuring the conductivity after every 0.1 mL NaOH

https://doi.org/10.1021/acs.biomac.4c01737
Biomacromolecules 2025, 26, 1372−1385

Scheme 1. Preparation of CNCs via Hydrothermally-Assisted MA Hydrolysis

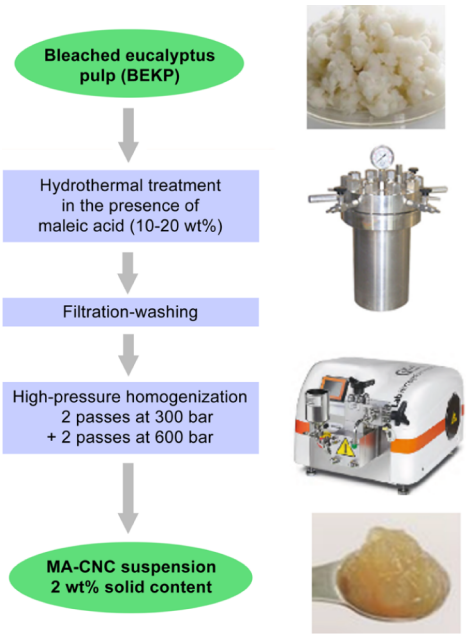

addition. The resulting titration trace was characterized by two equivalence points: the first one corresponded to the titration of the strong acid added to protonate the carboxylic group, and the second one corresponded to the titration of the weak acid groups. CC (in μmol g^{-1}) was then calculated as

$$CC = (V_2 - V_1) \times c/w \quad (1)$$

where V_1 and V_2 are the equivalent volumes of NaOH, in liters, c is the concentration of NaOH (0.01 M), and w is the dry weight of the sample.

2.5. Cellulose and Hemicellulose Contents. The cellulose content was determined according to the TAPPI 429 om-23 standard, and the hemicellulose content was determined by gravimetry after dissolution in a 24% KOH solution.

2.6. Degree of Polymerization (DP). The DP was measured by viscosimetry according to the ISO 5351:2010 standard. In a typical experiment, 20 to 60 mg of fibers, previously filtered in a 400-mesh nylon cloth and thoroughly washed, were solubilized in 10 mL of a 0.5 M cuproethylene diamine (CED) solution, leading to solutions within the 2 to 6 mg mL^{-1} range. The solubilization of the fibers was complete after 48 h. The intrinsic viscosity was measured in a capillary flow viscosimeter and was calculated from the specific and relative viscosity values, as reported elsewhere.[16] The viscosimetric average molecular weight DP_v was calculated as

$$\eta = K \times DP_v^a \quad (2)$$

where η is the intrinsic viscosity, in dL g^{-1}, and K and a are factors equal to 2.28 and 0.76, respectively.[17]

2.7. Transmission Electron Microscopy (TEM). A JEOL JEM 2100-Plus microscope operating at 200 kV was used to observe specimens prepared by depositing droplets of dilute CNC suspensions onto glow-discharged, carbon-coated copper grids and staining with 2 wt % uranyl acetate. Images were recorded with a Gatan Rio 16 camera.

2.8. Crystallinity. X-ray diffraction (XRD) profiles were recorded from strips of nanopapers in the case of BEKP and MA-CNCs, and a powder poured into a 1.0 mm (outer diameter) glass capillary in the case of CF-CNCs, using the Ni-filtered CuK radiation produced by a Philips PW3630 generator (30 kV, 20 mA, λ = 0.15418 nm). The profiles were normalized to the total diffracted intensity calculated by integrating the profile between 6 and 37°. A crystallinity index (CrI) was calculated according to Segal's formula:[18]

$$CrI = 100 \times \frac{I_C - I_A}{I_C} \quad (3)$$

where I_C is the maximum intensity of the 200 peak (contribution of the crystalline fraction) and I_A the intensity of the minimum between 18 and 19° (contribution of the amorphous fraction).

2.9. Fourier-Transform Infrared Spectroscopy (FTIR). The FTIR-ATR spectra were recorded from 500 to 4000 cm^{-1} using a PerkinElmer Spectrum II spectrometer equipped with a diamond crystal plate ATR MIR single-reflection accessory, with a resolution of 4 cm^{-1}.

2.10. Thermogravimetric Analysis (TGA). The thermal stability of the samples was analyzed with a TGA 400 thermogravimetric analyzer (PerkinElmer) using about 10 mg of solid samples heated at a temperature ranging from 30 to 800 °C and a heating rate of 10 °C min^{-1} under airflow.

2.11. Rheological Measurements. The rheological measurements were performed at 25 °C using a stress-controlled rheometer (Kinexus Pro+, Malvern Instruments, U.K.) equipped with a cone−plate geometry (cone angle: 2°, diameter: 20 mm, truncation: 56 μm). The tests in dynamic mode began by identifying the linear viscoelastic region through measurements of the storage modulus (G') and loss modulus (G'') as a function of strain. A frequency sweep was then conducted at a fixed strain within this linear domain. The steady-state shear viscosity was assessed at shear rates ranging from 0.1 to 100 s^{-1}. To prevent sample slippage, the surfaces of the tools were roughened by using sandpaper.

2.12. Particle Size and ζ-Potential Measurements. The particle size distribution and surface charge of the CNCs were measured by dynamic light scattering (DLS) with a Zetasizer ZS instrument from Malvern at 25 °C. The suspension was kept at around 0.2 wt % concentration, with pH controlled using NaOH/HCl (10^{-3} M). Each measurement was performed in triplicate.

2.13. Nanocomposites Processing. A commercial acrylic latex (S330 from MPC-Prokim-Tunisia), poly(styrene-*co*-butyl acrylate) with a monomer ratio of 60/40 wt %, was used as a matrix. The particle size of the latex, solid content, and glass transition temperature of the latex were 200 nm, 50 wt %, and 15 °C, respectively. The nanocomposite films were prepared by mixing the latex with the appropriate amount of CNC suspension for 30 min, followed by casting the mixture in a Teflon mold and drying at 40 °C for 6 h. A transparent film was obtained after complete drying, with a thickness of 200 to 300 μm.

2.14. Dynamic Mechanical Analysis. Dynamic mechanical analysis (DMA) was carried out in tension mode using PYRIS Diamond DMA (PerkinElmer, Waltham, MA) under heating at 2 °C min^{-1}, at a vibration frequency of 1 Hz. The storage (E') and loss (E'') moduli were measured as a function of temperature.

2.15. Tensile Tests. Tensile tests were conducted using a universal testing machine (TM2101 V4.23) equipped with a cell load of 500 N. Experiments were performed at room temperature at a rate of 10 mm min^{-1}.

2.16. Aqueous Biodegradation Conditions. The biochemical oxygen demand (BOD) was evaluated according to the EN ISO 14851 method[19] by measuring the oxygen demand in a closed respirometer under aerobic conditions at 30 °C using OxiTop vessels. CNCs were dried into thin films and cut into small fragments, while fibers were used as such in the dry form. About 100 mg of each material was placed in an autoclaved cultivation bottle with an internal volume of 1 L each in the presence of a 400 mL mineral solution[19] and 1 mL of activated sludge from a local urban wastewater treatment plant. The sealed bottles were placed for 30 days in an incubator maintained at 25 °C under magnetic stirring, and the BOD was measured daily. Three bottles containing the inoculum solution were prepared without the substrate as a control. Two grams of soda lime containing NaOH was placed in the upper body of the bottle as a CO_2

https://doi.org/10.1021/acs.biomac.4c01737
Biomacromolecules 2025, 26, 1372−1385

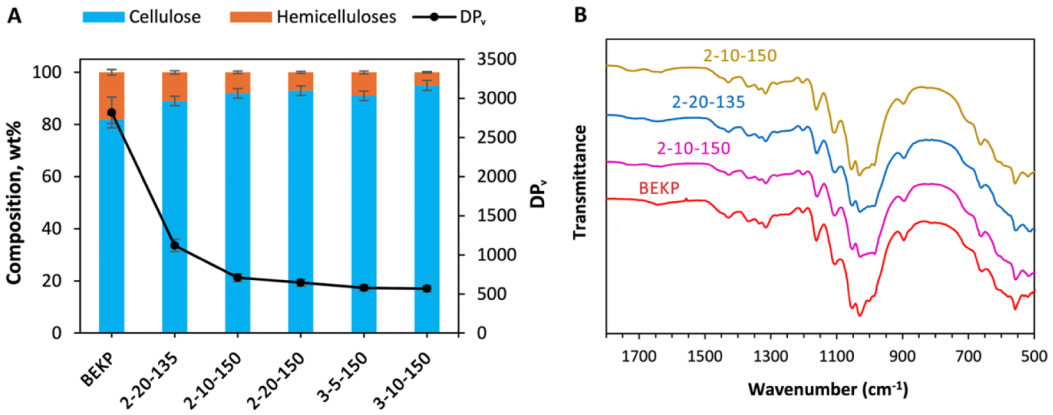

Figure 1. Chemical composition and DP_v (A), and FTIR spectra (B) of the bleached fibers after hydrothermal pretreatment under different conditions.

Table 1. Chemical composition, Carboxyl Content, Fine Percentage, Average Length, and DP_v After Hydrothermal Pretreatment at Different Conditions[ab]

Sample t-M-T[a]	CC (μmol g^{-1})	Cellulose (wt %)	Hemicelluloses (wt %)	DP_v	Average length (μm)	Fines[b](wt %)
BEKP	56	82	18	2820	850	5
2-20-135	208	92	11	1120	280	57
2-10-150	274	92	8	710	310	61
2-20-150	285	93	7	645	240	68
3-5-150	189	91	9	578	420	51
3-10-150	240	95	5	567	220	56

[a]t, M, and T stand for time (in h), MA concentration (in wt %), and temperature (in °C). [b]Fine content expressed as % in length.

absorber. Measurements were triplicated, and results were given with a ± 5% standard deviation.

The biodegradation percentage of samples was calculated as follows:

$$\text{Biodegradability}(\%) = \frac{\text{BOD}}{\text{ThOD}} \times 100 \quad (4)$$

where the BOD was subtracted from the values of the samples obtained during the degradation activity, and the theoretical oxygen demand (ThOD) was calculated based on the chemical composition of cellulose.

3. RESULTS AND DISCUSSION

3.1. Hydrothermal Pretreatment of the Fibers in the Presence of MA. BEKP contained 82 wt % cellulose and 18 wt % hemicelluloses, respectively (Figure 1A), in agreement with previous works.[20] In all cases, the hydrothermal treatment (HT) resulted in a decrease in the hemicellulose content with increasing severity of the treatment (time, temperature, and MA concentration). For instance, the treatment at 135 °C for 2 h in the presence of 20 wt % of MA (2-20-135) resulted in a decrease of the hemicellulose content from 18 to 11 wt %, and a further reduction was observed under the same conditions but at a higher temperature (2-20-150), reaching 7%. The lowest hemicellulose content (around 5 wt %) was reached when the temperature was set at 150 °C for 3 h in the presence of 10 wt % MA, which was the most severe condition studied in this work. This marked decrease in hemicellulose content is the consequence of the HT, which resulted in the hydrolysis of hemicelluloses that were dissolved in water. The degradation of hemicelluloses during HT is well documented in the literature for bleached pulp, as well as neat wood chips[21,22] where the hydrolysis usually results in short chains that are solubilized during HT.[23] This procedure is used industrially to produce dissolving pulps with high cellulose content intended for the fabrication of viscose fibers for textile production,[24] where the highest cellulose content is required. The hydrolysis of hemicelluloses was favored and easier under hydrothermal conditions than that of cellulose because of the amorphous and heterogeneous structure of hemicelluloses and lower degree of polymerization, which, in turn, promoted accessibility of the hydrolyzing agents.[17]

The FTIR spectra of the fibers after HT did not reveal any noticeable evolution compared with the neat pulp (Figure 1B). Only a minor change was noted, corresponding to a decrease in the intensity of the band located at 1030 cm^{-1}, typical of hemicelluloses, and a relative increase in the intensity of the band at around 1720 cm^{-1}, typical of CO groups. This may be attributed to the overlapping of the cellulose bands with those of hemicelluloses. The typical bands of cellulose appeared at 895 cm^{-1} (C−H deformation vibrations), 1020 and 1050 cm^{-1} (C−O stretching), 1110 and 1155 cm^{-1} (C−O−C ring-stretching vibration), 1200 and 1230 cm^{-1} (C−OH in-plane bending), 1265 cm^{-1} (C−H bending), 1314 cm^{-1} (C−H_2 wagging), 1332 cm^{-1} (C−OH in-plane bending), 1366 cm^{-1} (C−H bending), and 1421 cm^{-1} (C−H_2 symmetric bending). The relative increase in intensity of the CO band at 1720 cm^{-1} is presumably due to the esterification of a fraction of hydroxyl groups of cellulose induced by MA. This also explains the increase in the carboxyl content (CC) of the fibers after the HT. However, the CC under different HT conditions remained roughly around 200−250 μmol g^{-1} and did not significantly change by increasing the MA concentration or the temperature. This implies that, surprisingly, less than 2 wt % of the initial MA was esterified with the available hydroxyl groups. Considering the equilibrium character of the esterification reaction between MA and the hydroxyl groups from cellulose

https://doi.org/10.1021/acs.biomac.4c01737
Biomacromolecules 2025, 26, 1372−1385

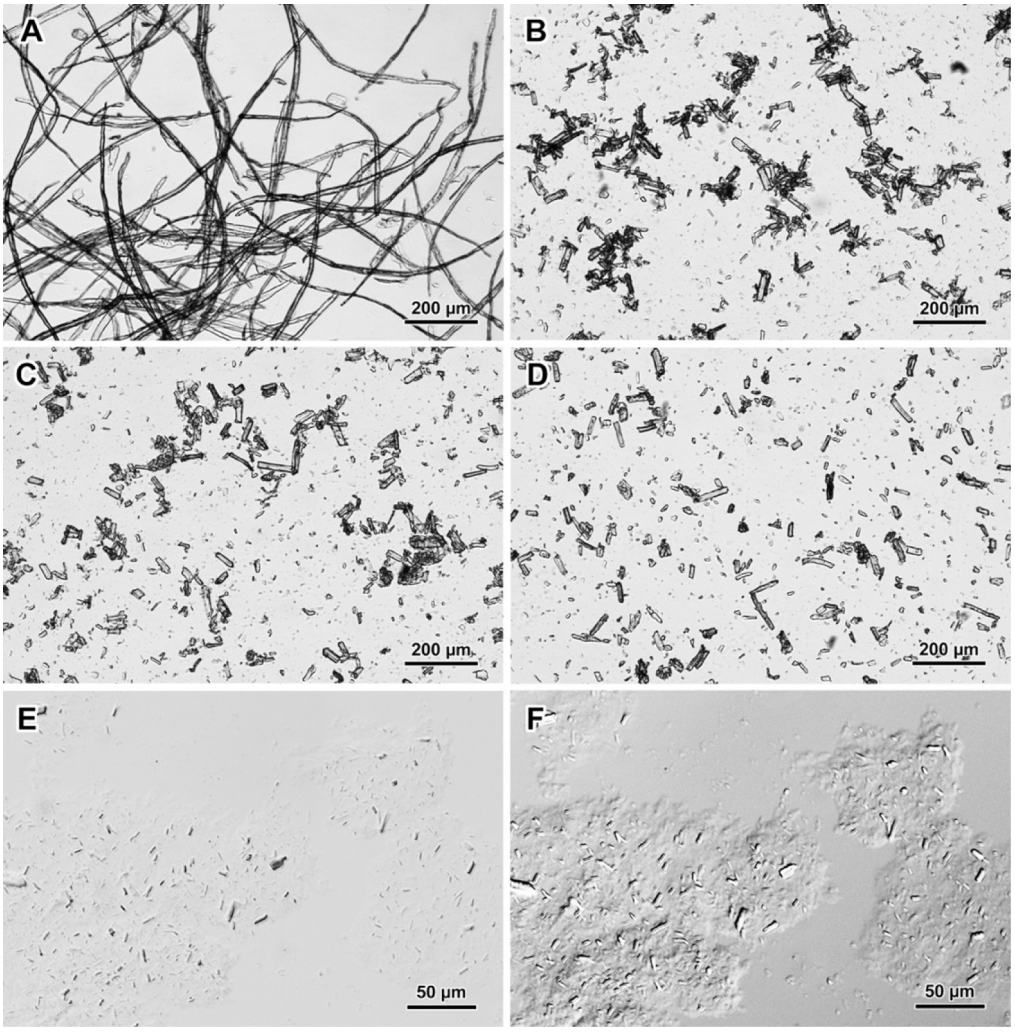

Figure 2. Optical micrographs of neat BEKP fibers (A), HT-treated fibers corresponding to samples 2-20-135 (B), 2-10-150 (C), and 3-10-150 (D); (E,F) CNC gel from sample 2-10-150. Image (F) corresponds to the same area as image E but was recorded in differential interference contrast.

and hemicelluloses, with an equilibrium constant lower than 4,[25] this would inevitably result in the grafting of MA on cellulose and hemicelluloses via an esterification reaction. Another reason that likely contributed to the low CC might be the preferential esterification of hydroxyl groups from hemicelluloses compared with those of cellulose. This phenomenon was favored by the amorphous character of hemicelluloses, allowing higher accessibility of their hydroxyl groups to MA. However, given that a significant fraction of hemicelluloses was dissolved during the HT, this would contribute to preserving the CC.

The HT treatment imparted a significant effect on the DP_v of the fibers, resulting in a decrease of around 80% for the 3-10-150 sample, which corresponded to the more severe conditions. For all samples, the fibers experienced a significant decrease in DP_v with an increasing severity of the HT treatment in terms of temperature, time, and MA concentration (Table 1). For example, DP_v decreased from 2820 (BEKP) to 1120 after an HT treatment at 135 °C during 2 h (2-20-135), and to 645 when the temperature was increased to 150 °C while maintaining the treatment time and MA concentration (2-20-150). This effect of temperature was often reported for biomass and bleached cellulose fibers exposed to HT.[26] The decrease in DP_v is due to the cleavage of glycosidic bonds in the cellulose chains and the consequent reduction of their DP_v. This effect is the result of the particular conditions of HT treatment. Indeed, at elevated temperatures, the physical properties of water molecules were different from ambient liquid water in that hydrogen bonding in water became weaker and less persistent, due to the decrease in the dielectric constant.[27] As the dielectric constant of water decreases, it became less polar and more favorable for dissolving organic compounds that did not dissolve well in pure water. In addition, the kinetics of cellulose hydrolysis was highly influenced by the temperature, mainly over the kinetic constant of the hydrolysis reaction, but also over the activity factor due to the heterogeneous character of the suspension.[28] These conditions favored the diffusion of water molecules inside the micropores of the cellulose fibers and induced bond cleavage and depolymerization of the cellulose backbone. The presence of MA further promoted the hydrolysis by providing additional H_3O^+ species that are known to catalyze the cleavage of the glycosidic bond.[29]

The HT treatment significantly affected the morphology of the fibers, as was revealed by the optical microscopy images (Figure 2). The neat flexible BEKP fibers had a length-

https://doi.org/10.1021/acs.biomac.4c01737
Biomacromolecules 2025, 26, 1372−1385

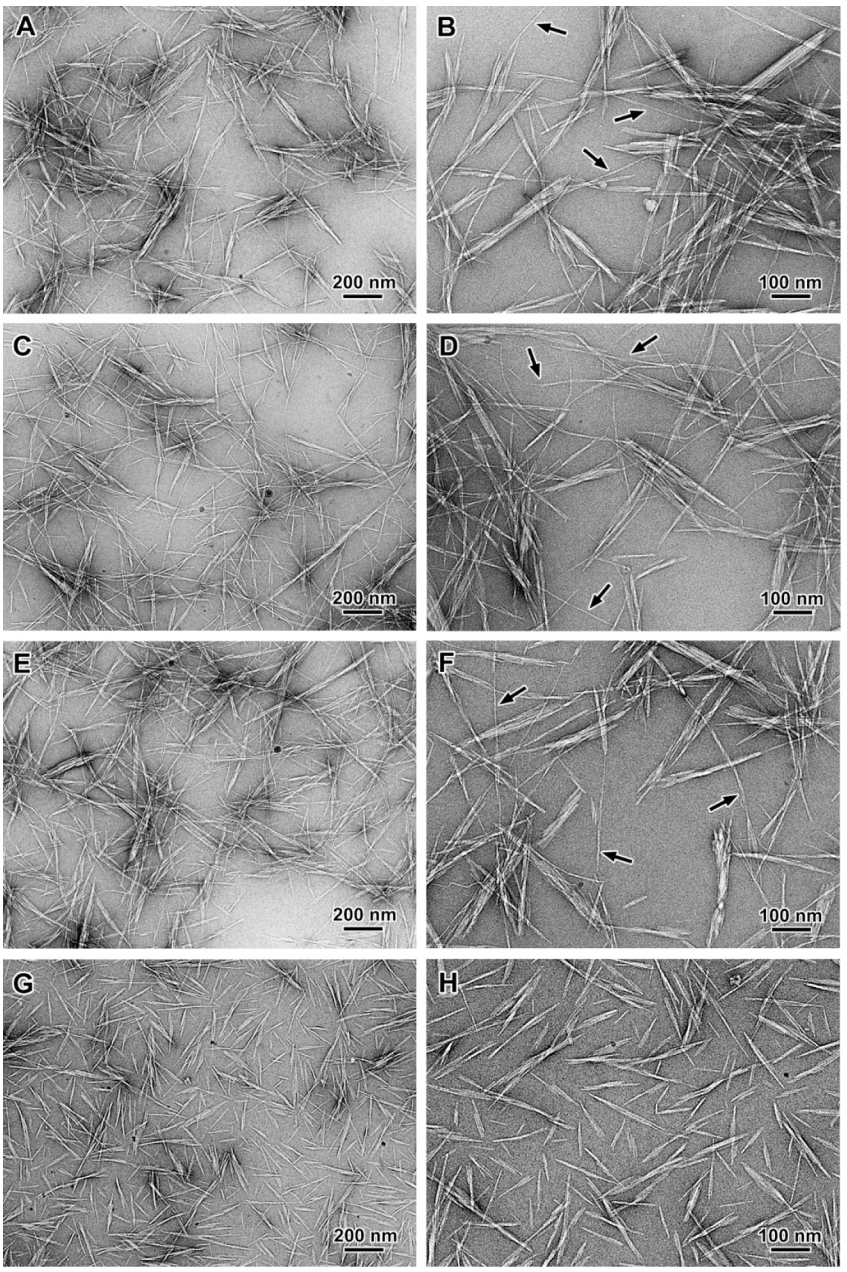

Figure 3. TEM images of negatively stained preparations from dilute suspensions from HT/HPH-treated fibers: (A,B) 2-20-135, (C,D) 2-10-150, (E,F) 3-10-150, and (G,H) CF-CNCs. The arrows point at some long and thin nanofibrils.

weighted average length of 850 nm, a width of 16 μm, and a coarseness of 0.087 mg m^{-1}, representing the linear mass. As expected, the fine content accounted for 5.5% in length, which is the typically reported value for unrefined *Eucalyptus globulus* bleached kraft pulp.[30] The HT treatment resulted in a marked decrease in fiber length to 300 and 220 μm for the 3-5-150 and 3-10-150 samples, respectively. Coarseness reached values of 0.40 and 0.18 mg m^{-1}, respectively, whereas the fine content also experienced a remarkable increase, accounting for 61 and 56%, respectively. This indicated that HT treatment induced significant fragmentation in length, while the width was preserved. This effect can be attributed to the huge decrease in the DP_v of the cellulose, which inevitably resulted in a weakening of the structural integrity of BEKP fibers.

3.2. CNCs from HT-Treated Fibers and High-Pressure Homogenization. CNCs were prepared by subjecting the HT-treated fibers to HPH for two cycles at 300 bar and two cycles at 600 bar. Immediately after the second pass at 300 bar, the fiber suspension exhibited a gel-like aspect, experiencing a remarkable thickening after the two additional passes at 600 bar. This indicates the successful breakdown of the HT-treated fibers into nanostructured objects with a high surface area and capacity to retain water. All homogenized samples exhibited a translucent gel-like aspect, with a white to yellowish color, depending on the HT conditions (Figure S1). The yellowish color of MA-CNC was primarily observed at a hydrothermal temperature of 150 °C, though the intensity of the color was not reproducible. We believe this yellowish hue arises from oxidized products or residual byproducts from the decomposition of hemicellulose, such as furfural and HMF (hydroxymethylfurfural), which are known to form during the hydrothermal treatment of hemicellulose. These derivatives

https://doi.org/10.1021/acs.biomac.4c01737
Biomacromolecules 2025, 26, 1372−1385

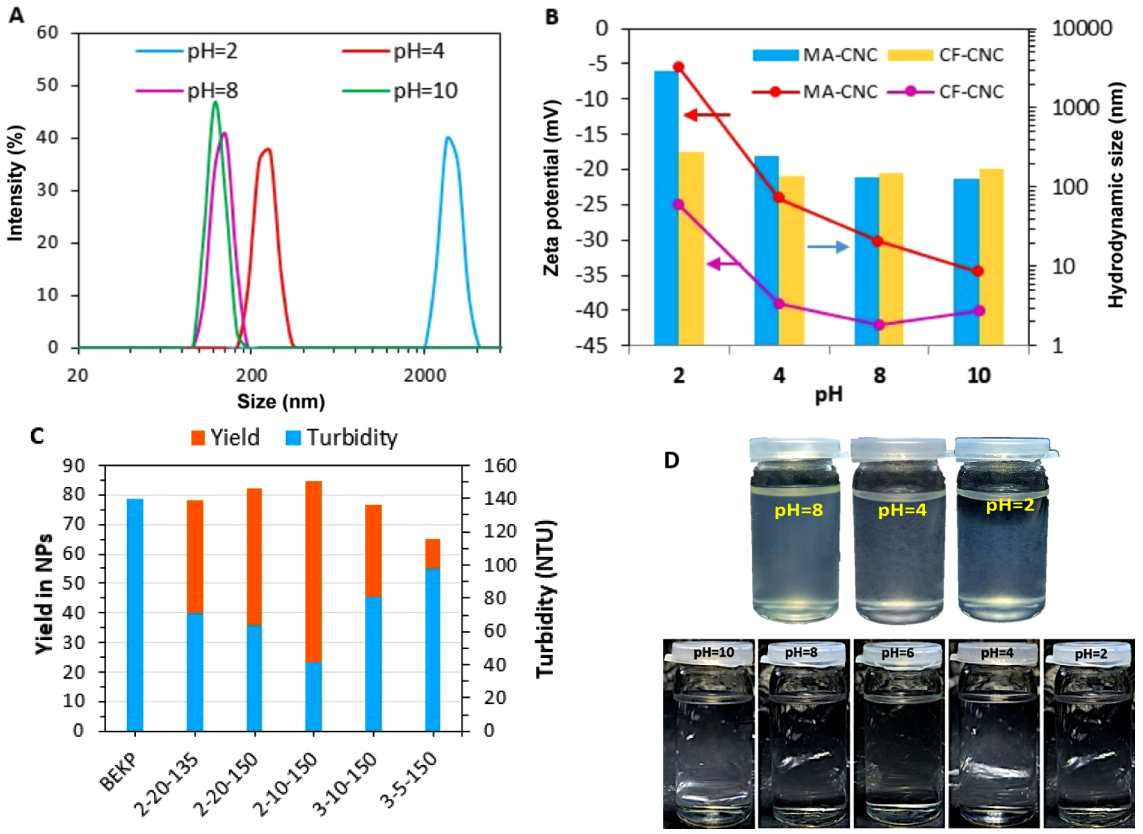

Figure 4. Colloidal properties of the obtained CNCs compared to CF-CNCs: (A) Size distribution by DLS analysis; (B) ζ-potential and hydrodynamic size as a function of pH; (C) yield and turbidity of CNC suspension from different HT samples; (D) visual aspect of several 0.5 wt % CNC suspensions at different pH values. The top three correspond to 2-20-150 CNCs and the bottom ones to CF-CNCs.

are highly colored upon exposure to oxygen. However, based on the light yellowish color, we presume that these side products were present only in small amounts. It is worth noting that the color of the CNC suspension remained stable and showed no changes during storage, even for several months.

The optical micrographs of the HT-treated fiber reveal only sporadic residual fragments (Figure 2E,F) likely stemming from the presence of micrometer-sized particles that were not fully disintegrated.

The TEM images of negatively stained preparations from 2 to 20−135 (Figure 3A,B), 2-10-150 (Figure 3C,D), and 3-10-150 (Figure 3E,F) dilute suspensions looked qualitatively rather similar and revealed networks of different types of particles that could not be completely disentangled by dilution and mild sonication: several hundred nanometer-long slender nanofibrils and shorter but bulkier particles (typically 200−400 nm in length and 10−40 nm in width) composed of a few bundled elementary crystallites that were not fully separated by the hydrolysis and HPH treatments. By comparison, the CF-CNCs prepared by conventional acid hydrolysis were more homogeneous in size and individualization, mainly containing individual 50−200 nm long and 3−10 nm wide rodlike particles composed of 1-5 elementary crystallites (Figure 3G,H).

The colloidal properties of the CNC suspensions, in terms of their stability at different pH levels, surface charge, and rheology, were investigated by particle size distribution analysis using DLS, ζ-potential measurement, and dynamic rheology. The particle size distribution exhibited a monomodal distribution, the position of which varied with the pH (Figure 4A). Above pH 7, the size distribution shifted to the lowest range, with a maximum peaking below 150 nm. At decreasing pH, especially below pH 4, a shift to a higher size was observed, indicating the occurrence of aggregation of particles. This was also confirmed by the visual aspect of the suspension at different pH levels, where the CNC suspensions remained translucent up to pH 4 and turned hazy at pH lower than 4, and at pH 2, visible aggregation with the formation of coarse particles could be seen (Figure 4D). This evolution in both the aspect and size distribution could be explained by the changes that pH imparts on the surface charge of the CNCs, as outlined in Figure 4B. At basic pH (i.e., 8 and 10), the suspensions exhibited a negative ζ-potential, with an absolute value exceeding 25 mV, which is enough to ensure colloidal stability through electrostatic repulsion-stabilization. As the pH decreased, the absolute value of the ζ-potential decreased to −5 mV at pH 2, close to the isoelectric point, promoting aggregation. This evolution in the ζ-potential can be attributed to the presence of carboxylic groups, induced by the esterification of MA on the surface of the CNCs, which appear in their protonated form at acidic pH levels, and in their sodium salt form as the pH increases. Conversely, in the case of commercial CNCs produced by acid hydrolysis, the changes in the ζ-potential were lower, ranging from −40 to −25 mV at decreasing pH, while the particle size distribution remained almost constant around 300 nm for all of the explored pH range. This difference in behavior against pH changes can be attributed to the presence of the sulfate half-ester groups (SO_4^-) on the surface of CNCs, which remained fully ionized

https://doi.org/10.1021/acs.biomac.4c01737
Biomacromolecules 2025, 26, 1372−1385

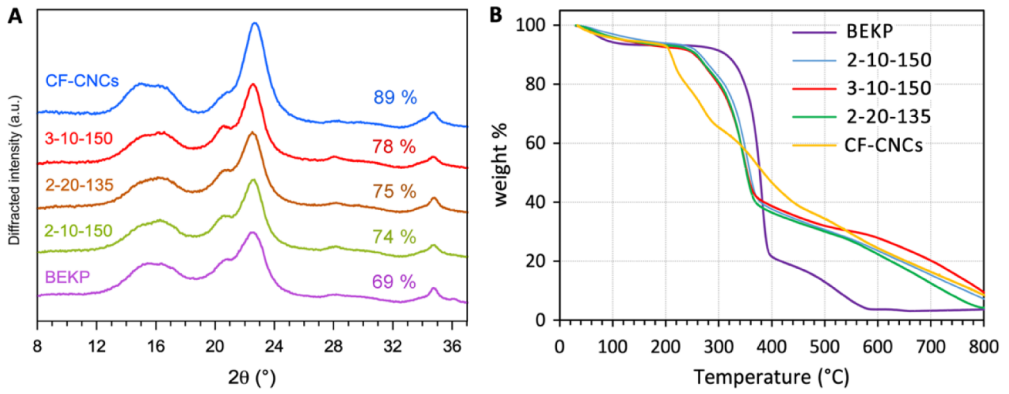

Figure 5. XRD profiles (A) and TGA traces (B) of neat BEKP, CNCs, and CF-CNCs. The crystallinity index is indicated above each XRD profile.

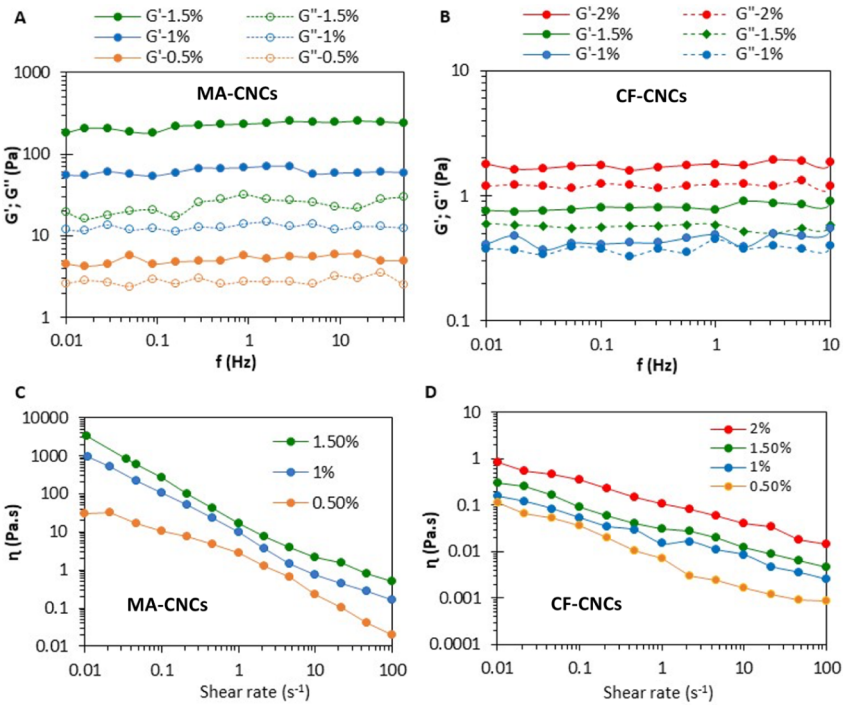

Figure 6. Rheological Analysis of MA-CNCs and CF-CNCs: Frequency sweeps of *G'* and *G"* at different solid contents of (A) MA-CNCs from 2 to 20-150 (B) CF-CNCs, and the corresponding viscosity as a function of shear rate (C,D).

over this pH domain, bringing negatively charged groups over a wide pH range, which increased the absolute value of the ζ-potential keeping it far from the isoelectric point. The negative ζ-potential, remaining above 25 mV in absolute value, accounts for the high transparency of the CF-CNC suspension, even at a solid content of 1−2% (Figure 4D). In contrast, the MA-CNC suspension remained stable only at pH levels above 6, as evidenced by changes in its visual appearance (Figure 4D).

The yield, expressed as the nanosized fraction in the CNC suspensions, is another important parameter that should be considered. In the H_2SO_4 hydrolysis route, the maximum achievable yield varies between 20 and 40 wt %, depending on the acid concentration, hydrolysis time, and temperature.[31] The hydrolysis conditions in terms of acid concentration and time of hydrolysis should be optimized to avoid an excessive decrease in DP_v and CNC length due to the hydrolysis of the β-1,4 bonds and depolymerization. In the proposed approach involving the use of MA, a yield between 75 and 84 wt % was achieved at an MA concentration ranging from 10 to 20 wt % and HT between 2 and 3 h at 150 °C. The highest yield (84 wt %) was achieved in the presence of 10 wt % MA at 150 °C for 2 h (2-10-150). A similar yield was reported in the literature for organic acid hydrolysis.[32] However, unlike the works reported so far regarding the use of organic acids for hydrolysis at an acid concentration within the 50−70 wt % range, in this work, a significantly lower concentration of MA was enough to effectively hydrolyze the cellulose fibers over a reasonable processing time. Moreover, in all instances, a DP_v exceeding 500 was achieved, allowing for the preservation of a high aspect ratio for the CNCs. The high yield in CNCs (Figure 4B) accounts for the good clarity and optical aspect of the CNC suspension (at pH > 6) and the low turbidity (Figure 4B), mainly for the 2-10-150 and 2-20-150 CNCs.

The XRD profiles of the CNCs recorded from neat BEKP and pretreated fibers are shown in Figure 5A. Similar diffraction peaks appeared in all profiles. The $1\bar{1}0$ and 110 reflections overlapped into a broad peak centered at about 16°, while the peaks located at 20.6°, 22.6°, and 34.7° corresponded

https://doi.org/10.1021/acs.biomac.4c01737
Biomacromolecules 2025, 26, 1372−1385

Scheme 2. Schematic Sequence of the CNC Preparation by Hydrothermally-Assisted MA Hydrolysis

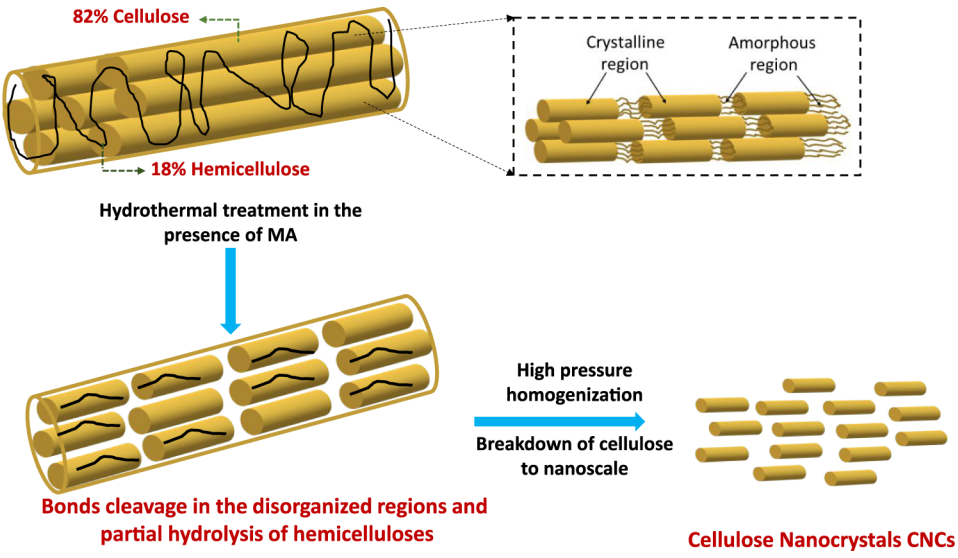

to reflections from the (102), (200), and (004) planes of cellulose Iβ, respectively.[33] Preferential orientations of the CNCs upon drying into thin films are known to influence the relative peak intensities in the XRD profiles of nanocelluloses. However, after comparison with the theoretical profile calculated by French,[33] we considered that the uniplanarity effect was small and did not significantly affect the CrI that was used to compare samples. Regardless of the pretreatment conditions, the CrI of the MA-CNCs was around 76%, which was higher than that of BEKP fibers (69%) but lower than that of CF-CNCs (89%) produced by conventional H_2SO_4 hydrolysis.

The thermal stability of the CNCs was also assessed by TGA under airflow and compared with the neat fibers and commercial CNCs (Figure 5B). The thermogram of the neat BEKP was characterized by an abrupt weight loss of more than 80% occurring between 300−400 °C, which was attributed to the thermal decomposition of hemicellulose and cellulose. A shift to a lower temperature of the onset of thermal (T_{onset}) degradation was observed for the CNCs obtained by MA-hydrolysis as well as the commercial ones. The T_{onset} for all CNCs produced in this study was found to be around 260 °C and did not change with the treatment conditions, while a T_{onset} of around 200 °C was observed for CF-CNCs. This reveals a higher thermal stability of the obtained CNCs compared with those available commercially and obtained by H_2SO_4 hydrolysis. This superior thermal stability was also pointed out in other works, where a T_{onset} between 250 and 300 °C was reported.[34] The sensitivity of CNCs from H_2SO_4 hydrolysis to thermal degradation is well-known and is one of the shortcomings of CNCs, particularly for the melt-processing of the CNCs with polymer matrices. This poor thermal stability results from the presence of sulfate groups, which require less energy to dissociate, and the release of sulfuric acid during the degradation process that further catalyzes the depolymerization of cellulose.[5]

The rheological behavior of the CNC suspensions was studied by oscillatory sweep measurements of the storage modulus (G') and loss modulus (G'') as a function of frequency (f) in the linear domain (Figure 6A,B), and by shear-rate measurement of the η. The data for the MA-CNC suspensions at different solid content (SC) obtained from sample 2-10-150 are provided in Figure 6A,C. From 0.5 to 1.5 wt % SC, G' was higher than G'', with a G'/G'' ratio increasing with increasing SC. This indicates that, over 0.5 wt %, the MA-CNC suspension exhibited a gel-like character, with enhanced stiffness as SC increased. The gel-like character became visible over 1 wt %, as the G' reached values above 50 MPa, which is enough for the suspension to demonstrate a visible gel aspect at rest. The gel-like character indicates the generation of a connected network of CNCs, preventing the flow due to the limited mobility of the CNCs. The presence of long nanofibrils, in the case of MA-CNCs in addition to rodlike CNCs, may explain the shear thinning behavior of the MA-CNC suspensions, with increasing SC, and the marked gel-like character over 1 wt % SC. A different tendency was observed for CF-CNC suspensions where, at the same SC, a much lower G' was reached (about 100 times lower), and even at 2 wt % SC, the CNC suspension easily flowed without any sign of gel-like behavior at rest. The different behaviors of the suspensions, particularly regarding gel formation, can be attributed to variations in surface charge and the resulting electrostatic interactions, as well as differences in particle morphology. Specifically, the lower surface charge of MA-CNCs compared to that of CF-CNCs results in reduced electrostatic repulsion between the CNCs, promoting interactions among the CNCs through hydrogen bonding. Additionally, the presence of nanofibrils in the MA-CNC suspensions may contribute to particle entanglement, restricting the mobility of the CNCs and reinforcing the elastic properties of the suspension. This explains the gel-like nature of the MA-CNC suspension at concentrations above 1 wt % SC.

A power-law relationship of G' as a function of SC ($G' = K \times SC^n$) was found for both CNC suspensions, with exponent factors around 3.4 and 2.5 for MA-CNCs and CF-CNCs, respectively (Figure S3). The rheological behavior of CNCs prepared by H_2SO_4 hydrolysis is expected to change with the solid content, evolving from an isotropic to a biphasic structure, to reach a liquid crystalline state and, finally, a gel-like structure.[35]

https://doi.org/10.1021/acs.biomac.4c01737
Biomacromolecules 2025, 26, 1372−1385

The steady-state viscosity as a function of the shear rate for CNC suspensions was characterized by a steady decrease in viscosity, indicating shear-thinning behavior. This evolution is explained by the breakage of the CNC network and the alignment of the particles along the shear direction, causing a decrease in the interaction between CNCs. For 1 and 1.5 wt % MA-CNCs, the viscosity decreased as $\eta \approx \dot{\gamma}^{-1}$, within the range of shear rate ($\dot{\gamma} < 10\ s^{-1}$), meaning that the shear stresses (τ) tended to a constant value at low shear rates, which corresponds to the yield stress. The presence of a yield stress was confirmed from the evolution of τ vs $\dot{\gamma}$ (Figure S4), and was consistent with the oscillatory test measurements, revealing a much higher G' than G'' (Figure 6A,B). In the case of CF-CNCs, although a similar shear-thinning behavior was observed, the viscosity at a given solid content $\dot{\gamma}$ was much lower than for MA-CNCs. Moreover, for $\dot{\gamma} < 10\ s^{-1}$, η showed a power-law dependence with $\dot{\gamma}(\eta = K\dot{\gamma}^{-n})$ rate with n around 0.45.

3.3. Mechanism of the Production of CNCs via Hydrothermally Assisted Maleic Acid Hydrolysis. The hydrolysis effect of MA was not found to be sufficient to successfully disassemble cellulose fibers into CNCs, requiring a subsequent stage consisting in applying mechanical energy to disintegrate the treated fibers. The significant catalyzing action of HT is related to the change in the properties of water at high temperatures and pressure. Under hydrothermal conditions (i.e., at temperatures above 120 °C), water exhibits a lower dielectric constant, weaker and less persistent hydrogen bonds, and higher diffusivity because of the reduced extent of the hydrogen bond network.[27] These effects promote the diffusion of water molecules inside the cellulose fibers, which induces: (i) the weakening of the interfibrillar interaction, (ii) a hydration and swelling of the fibers, (iii) the depolymerization and dissolution of hemicelluloses, and (iv) the cleavage of the glycosidic bonds in the disorganized regions of the elementary nanofibrils. In turn, the presence of MA further promoted the depolymerization and dissolution of hemicelluloses and disorganized regions by catalyzing the hydrolysis of the glycosidic bonds. The resulting cleavage of the disorganized domains promoted the release of shorter particles during HPH (Scheme 2).

3.4. Biodegradation of CNCs in Aqueous Environment. To evaluate the biodegradability of CNCs in aqueous environments, the BOD method was adopted by monitoring the oxygen consumed by microorganisms while breaking down organic matter in water over a specified period. This standardized method, widely used for assessing the biodegradation of chemicals in sewage water and effluents,[36] has been successfully extended to polymers[37,38] and biobased nanoparticles[39] to evaluate their biodegradation in aquatic media, and is carried out in a closed inoculated respirometer vessel using the BOD OxiTop system.

Figure 7 illustrates the BOD biodegradation over 30 days for BEKP, MA-CNC, and CF-CNC. In the presence of inoculum, the biodegradation of all materials increased over time, reaching 16% for BEKP, 23% for MA-CNC, and 26% for CF-CNC after 30 days of incubation. Interestingly, despite their highly crystalline character, we observe a higher tendency for biodegradation of CNCs compared to neat fibers. This result suggests that the high specific surface area of CNCs provides an advantage for bacterial growth and proliferation on the cellulose substrate, thereby promoting biodegradation,

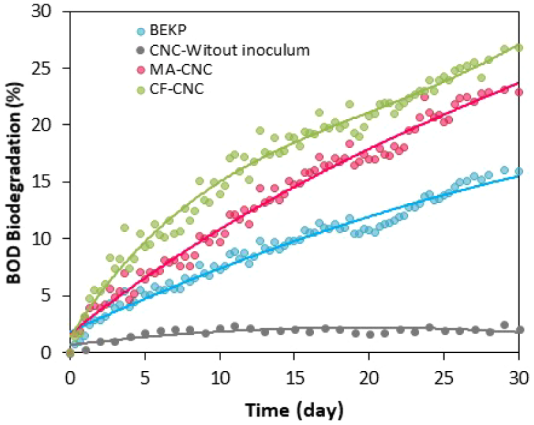

Figure 7. BOD biodegradation progression of neat BEKP and MA-CNCs in an aquatic medium at 30 °C.

while crystallinity has little effect on the process in an aquatic medium. This finding is in agreement with the recent work of Miyaji et al.,[40] who reported a similar trend and stated that biodegradability correlates with the specific surface area of the material. However, it is worth noting that in the absence of an inoculum rich in bacteria, no biodegradation of CNCs was observed over 30 days. This indicates that CNCs were resistant to biodegradation in water unless exposed to bacterial contamination.

3.5. Reinforcing Properties of MA-CNCs. One of the main attributes of CNCs is their strong reinforcing effect, especially when incorporated into a ductile polymer matrix, which can ensure appropriate distribution and successful polymer-CNC interactions. To investigate the reinforcement capacity of MA-CNCs, nanocomposite films were prepared by mixing the CNC suspension in different amounts with a waterborne polymer dispersion, followed by film formation by casting. The mechanical properties of the film were studied by DMA and a tensile test at 25 °C.

Figure 8A,B illustrates the evolution of E' with temperature for composite films reinforced with different MA-CNC and CF-CNC contents. In the absence of CNCs, the E' evolution of the neat polymer matrix exhibited the typical behavior of an amorphous polymer, with a transition from the glassy to a rubbery state between 20 and 30 °C, accompanied by a marked decrease of E' (about 3 orders of magnitude) and by a maximum in the tan δ plot (Figure S5). With the addition of CNCs, a steady increase of E' was observed, particularly in the rubbery state, while only a modest effect was noted in the glassy region. This enhancement is aligned with the expected properties of CNCs that reinforce and stiffen polymer matrices in the rubbery state, assuming their proper dispersion in the matrix.[41] The reinforcing effect of CNCs in composite materials is well documented and results from their specific attributes, namely (i) a high aspect ratio, a high crystallinity degree, and surface smoothness, which accounts for their unusually high modulus (130 GPa),[42] (ii) their ability to form percolated networks over a critical threshold, held by hydrogen bonding,[5] and (iii) their role in preventing fracture propagation, thereby increasing the material toughness and durability, while increasing the tear index of the polymer matrix.

As shown in Figure S5, the inclusion of CNC resulted in a continuous drop in the magnitude of the α relaxation, along with a shift toward lower temperatures of the peak. However, it

https://doi.org/10.1021/acs.biomac.4c01737
Biomacromolecules 2025, 26, 1372−1385

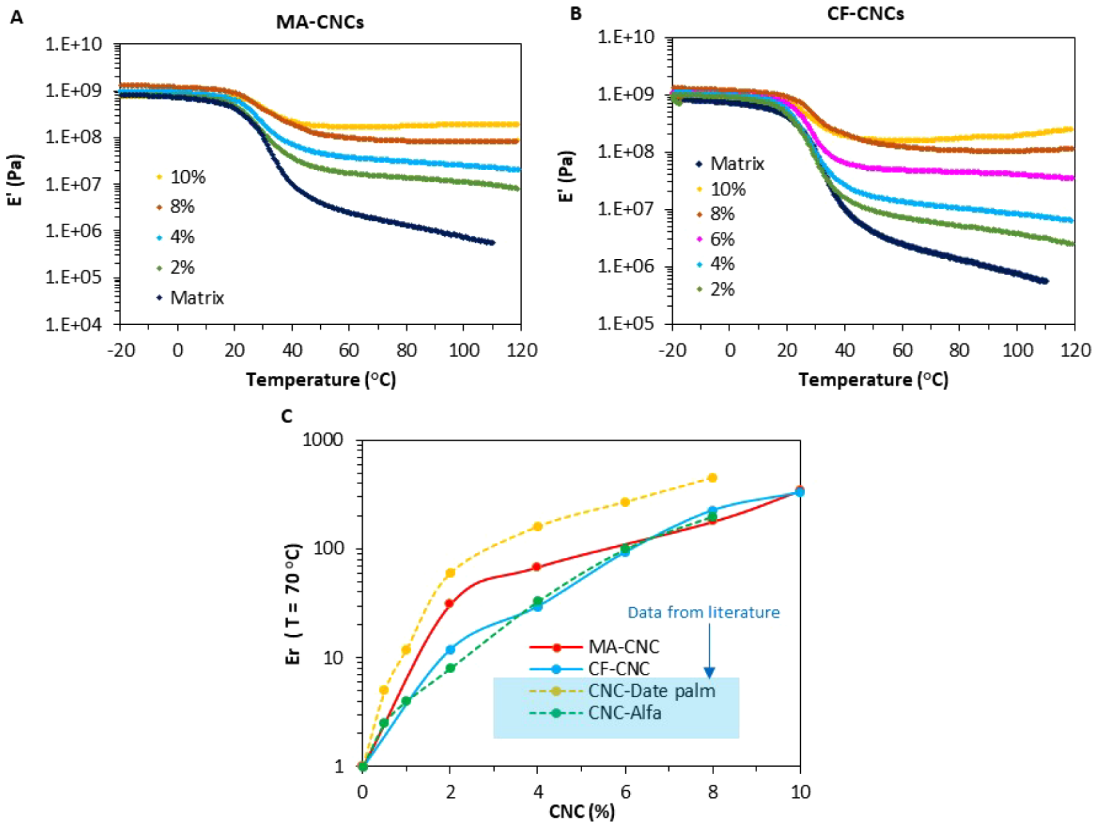

Figure 8. Evolution of the storage tensile modulus (E′) with testing temperature for different MA-CNCs from 2 to 20−150 (A) and CF-CNC composites (B), and effect of increasing CNC content over the relative modulus (E_r) (C).

is worth noting that this is likely a simple coupling effect and does not correspond to a shift in the glass transition temperature, as was highlighted in the literature.[41]

When comparing the evolution of the relative modulus $E_r = \frac{E'_{man}}{E'_{mat}}$ (with E'_{nan} and E'_{mat} being the storage modulus of the nanocomposite and unfilled matrix, respectively, measured in the rubbery region at 70 °C) with the CNC content for both types of CNCs (Figure 8C), it can clearly be seen that at a content below 6 wt %, MA-CNC-reinforced composites exhibited a higher E_r than those reinforced with CF-CNCs. However, over this level, both types of CNCs induced a nearly similar stiffening effect. This indicates that, at an equivalent CNC content below 6 wt %, MA-CNCs imparted a higher stiffening effect than CF-CNCs, resulting in lower effects on physical properties such as density.

For comparison purpose, data collected from the literature for nanocomposites prepared using CNCs from Alfa and date palm differed by their aspect ratio (the former has an aspect ratio of 10−15, while it is in the range of 35−40 for the latter). A similar polymer matrix was used for this work, and the relative modulus extracted was determined at the same temperature of 70 °C.

The reinforcing effect of CNCs was also explored through stress−strain behavior, which has the merit of assessing the strength of the material under the effect of nonlinear deformation. The stress−strain plots for the nanocomposite films at different CNC contents are shown in Figure 9, from which the tensile modulus (E) and ultimate strength (US) were extracted (Figure 9C,D). At increasing content of CNCs, an increment in E and US was observed in both types of CNCs, indicating an increase in the stiffness and strength of the film. However, as noted by DMA results, MA-CNCs achieved better enhancement in E and US than CF-CNCs.

Referring to literature data, four parameters are likely to affect the reinforcing potential in nanocomposites based on CNC nanofiller and a ductile matrix, namely, (i) the aspect ratio of CNC, (ii) their dispersion degree within the polymer matrix, (iii) their content in the matrix, and (iv) the crystalline degree of the nanofiller. In the present work, we attributed the difference in the reinforcing effect of two types of CNCs to the morphological difference between MA-CNCs and CF-CNCs, more specifically, to a difference in the length of the CNCs.

One might question the novelty of the present work compared with previous studies on preparing CNCs via the MA acid hydrolysis route. Indeed, this work provides several key advancements: First, it is the first to prepare CNCs using MA hydrolysis at a low concentration (10−20 wt %), whereas earlier studies typically used concentrations above 50 wt %. Second, we achieved a CNC yield exceeding 70 wt %, which is notably higher than that in previous works. Third, our approach eliminated the need for a centrifugation separation process. Finally, we introduced a hydrothermal treatment step to improve the efficiency of the hydrolysis process. This modification proved to be a key factor in facilitating the release of nanocellulose during organic acid hydrolysis.

Regarding the toxicity of MA, it is important to note that MA is a dicarboxylic acid widely used in industrial chemistry, particularly in the production of resins and polymers. MA can irritate the nose, throat, and lungs, causing symptoms such as coughing and wheezing, especially when inhaled. To minimize

https://doi.org/10.1021/acs.biomac.4c01737
Biomacromolecules 2025, 26, 1372−1385

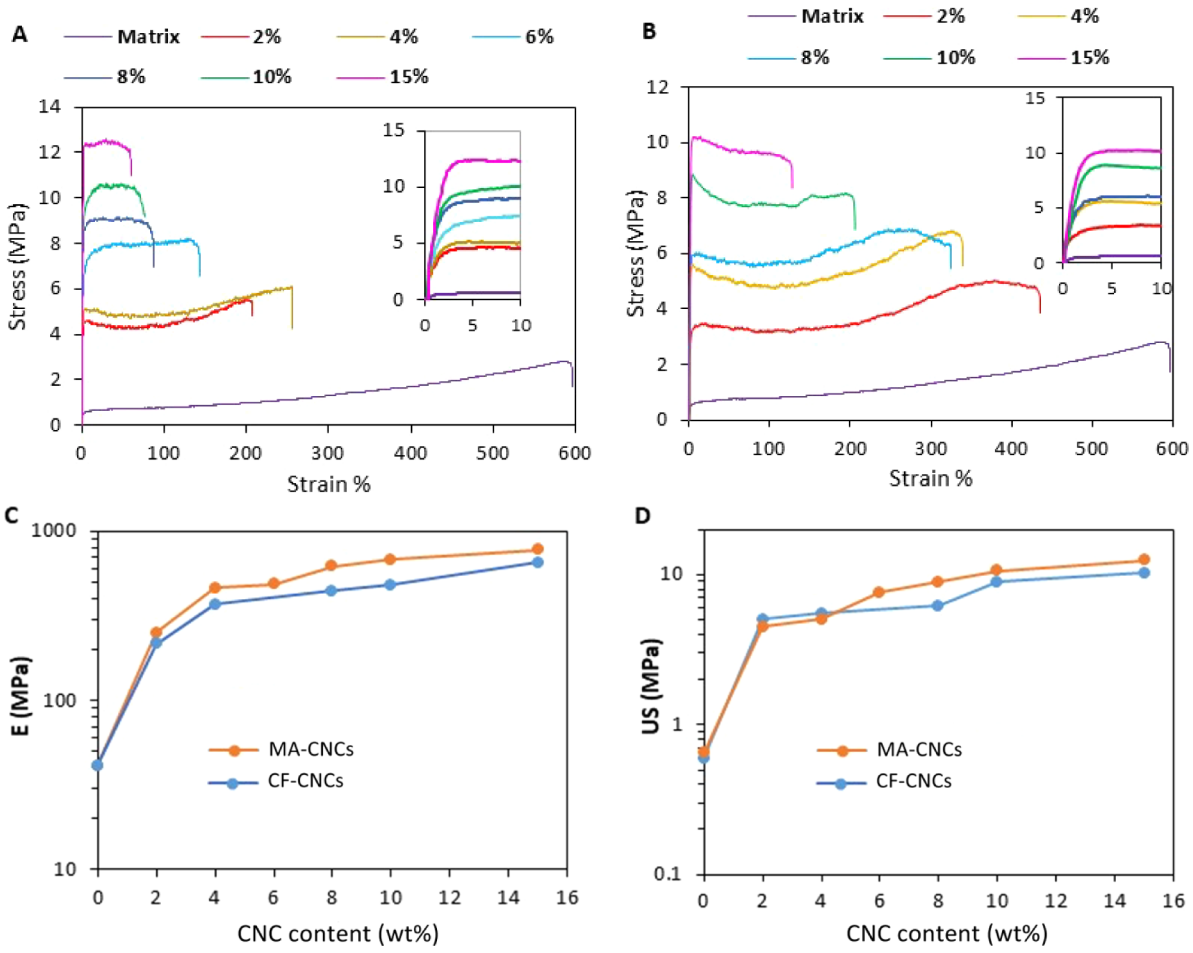

Figure 9. Stress−strain curves of the neat matrix and nanocomposite films at different CNC contents for MA-CNCs (A) and CF-CNCs (B), and the tensile modulus (C) and ultimate strength (D) of the nanocomposites.

potential toxicity risks, it is recommended to handle MA in the form of an aqueous solution rather than as a powder.

4. CONCLUSION

CNCs were produced at a high yield ranging from 70 to 85 wt % by HPH of hydrothermally treated BEKP fibers in the presence of 10 to 20 wt % maleic acid at 150 °C for 2 to 3 h. The resulting CNC suspensions exhibited a translucent to transparent gel consistency after undergoing 4 passes through the high-pressure homogenizer at pressures ranging from 300 to 600 bar. Remarkably, this gel was stable at pH 7−8 without any sign of syneresis or aggregation for over six months, attributed to the electrostatic stabilization conferred by carboxylic groups. TEM images confirmed the rodlike morphology of the CNCs, typically 200−400 nm in length and 10−40 nm in width. The comparative analysis with commercial-grade CF-CNCs demonstrated superior thermal stability of CNCs obtained via MA hydrolysis followed by HPH, with an onset of thermal degradation at 260 °C compared with 200 °C for CF-CNCs. Furthermore, nanocomposite films prepared by blending the CNC suspension with a waterborne latex, followed by casting and film formation at room temperature, revealed enhanced reinforcing effects of MA-CNCs compared with CF-CNCs, as evidenced by DMA and tensile tests.

Overall, our study presents a high-yield method for CNC preparation with excellent colloidal and thermal stability, employing fewer chemical reagents and steps compared with sulfuric acid hydrolysis. Notable distinctions from previous works include the utilization of lower MA concentrations (10−20 wt %) compared to the typically required concentrations exceeding 50 wt %, higher CNC yields exceeding 70 wt %, and the elimination of the need for centrifugation separation. These improvements were facilitated by adopting hydrothermal conditions, leveraging alterations in water properties under high temperatures and pressures to enhance the release of CNCs.

■ ASSOCIATED CONTENT

Supporting Information

The Supporting Information is available free of charge at https://pubs.acs.org/doi/10.1021/acs.biomac.4c01737.

Photos of the CNC gel prepared at different conditions, TEM images of CNCs prepared under different hydrothermal conditions, complement of the rheological analysis of the CNC gels, and the tan α versus temperature plots at 1 Hz for the nanocomposite films (PDF)

https://doi.org/10.1021/acs.biomac.4c01737
Biomacromolecules 2025, 26, 1372−1385

AUTHOR INFORMATION

Corresponding Author

Sami Boufi − *LMSE - Faculty of Science, University of Sfax, Sfax 3018, Tunisia;* orcid.org/0000-0002-3153-0288; Email: sami.boufi@fss.rnu.tn

Authors

Amira Najahi − *LMSE - Faculty of Science, University of Sfax, Sfax 3018, Tunisia;* orcid.org/0000-0001-7547-3281

Marc Delgado-Aguilar − *LEPAMAP-PRODIS Research group, University of Girona, Girona 61-17003, Spain*

Jean-Luc Putaux − *CNRS, CERMAV, Univ. Grenoble Alpes, Grenoble F-38000, France;* orcid.org/0000-0002-9760-5369

Complete contact information is available at: https://pubs.acs.org/10.1021/acs.biomac.4c01737

Notes

The authors declare no competing financial interest.

ACKNOWLEDGMENTS

The authors thank the NanoBio-ICMG Platform (UAR 2607, Grenoble) for granting access to the Electron Microscopy facility. CERMAV is part of Institut Carnot PolyNat (Investissements d'Avenir #ANR-11-CARN-030-01) and participates in the Glyco@Alps program (Investissements d'Avenir #ANR-15-IDEX-02).We also thank the Ministry of Higher Education and Research of Tunisia for financial support through Project 21P2ES-D6P3, and CMCU project: 23G1118.

REFERENCES

(1) Dufresne, A. *Nanocellulose: from nature to high performance tailored materials*; Walter de Gruyter GmbH & Co KG, 2017.

(2) Lin, N.; Huang, J.; Dufresne, A. Preparation, properties and applications of polysaccharide nanocrystals in advanced functional nanomaterials: a review. *Nanoscale* **2012**, *4* (11), 3274−3294.

(3) Kalashnikova, I.; Bizot, H.; Cathala, B.; Capron, I. New Pickering emulsions stabilized by bacterial cellulose nanocrystals. *Langmuir* **2011**, *27* (12), 7471−7479.

(4) Lin, N.; Dufresne, A. Nanocellulose in biomedicine: Current status and future prospect. *Eur. Polym. J.* **2014**, *59*, 302−325.

(5) Roman, M.; Winter, W. T. Effect of sulfate groups from sulfuric acid hydrolysis on the thermal degradation behavior of bacterial cellulose. *Biomacromolecules* **2004**, *5* (5), 1671−1677.

(6) Yu, H.; Qin, Z.; Liang, B.; Liu, N.; Zhou, Z.; Chen, L. Facile extraction of thermally stable cellulose nanocrystals with a high yield of 93% through hydrochloric acid hydrolysis under hydrothermal conditions. *J. Mater. Chem. A* **2013**, *1* (12), 3938−3944.

(7) Rosa, M.; Medeiros, E.; Malmonge, J.; Gregorski, K.; Wood, D.; Mattoso, L.; Glenn, G.; Orts, W.; Imam, S. Cellulose nanowhiskers from coconut husk fibers: Effect of preparation conditions on their thermal and morphological behavior. *Carbohydr. Polym.* **2010**, *81* (1), 83−92.

(8) Wang, Y.; Liu, H.; Wang, Q.; An, X.; Ji, X.; Tian, Z.; Liu, S.; Yang, G. Recent advances in sustainable preparation of cellulose nanocrystals via solid acid hydrolysis: A mini-review. *Int. J. Biol. Macromol.* **2023**, *253*, 127353.

(9) Chen, L.; Zhu, J.; Baez, C.; Kitin, P.; Elder, T. Highly thermal-stable and functional cellulose nanocrystals and nanofibrils produced using fully recyclable organic acids. *Green Chem.* **2016**, *18* (13), 3835−3843.

(10) Song, K.; Ji, Y.; Wang, L.; Wei, Y.; Yu, Z. A green and environmental benign method to extract cellulose nanocrystal by ball mill assisted solid acid hydrolysis. *J. Cleaner Prod.* **2018**, *196*, 1169−1175.

(11) Bondancia, T. J.; de Aguiar, J.; Batista, G.; Cruz, A. J.; Marconcini, J. M.; Mattoso, L. H. C.; Farinas, C. S. Production of nanocellulose using citric acid in a biorefinery concept: effect of the hydrolysis reaction time and techno-economic analysis. *Ind. Eng. Chem. Res.* **2020**, *59* (25), 11505−11516.

(12) Wang, R.; Chen, L.; Zhu, J.; Yang, R. Tailored and integrated production of carboxylated cellulose nanocrystals (CNC) with nanofibrils (CNF) through maleic acid hydrolysis. *Chem. Nano. Mater.* **2017**, *3* (5), 328−335.

(13) Bian, H.; Chen, L.; Dai, H.; Zhu, J. Effect of fiber drying on properties of lignin containing cellulose nanocrystals and nanofibrils produced through maleic acid hydrolysis. *Cellulose* **2017**, *24*, 4205−4216.

(14) Bian, H.; Chen, L.; Dai, H.; Zhu, J. Integrated production of lignin containing cellulose nanocrystals (LCNC) and nanofibrils (LCNF) using an easily recyclable di-carboxylic acid. *Carbohydr. Polym.* **2017**, *167*, 167−176.

(15) Besbes, I.; Vilar, M. R.; Boufi, S. Nanofibrillated cellulose from alfa, eucalyptus and pine fibres: preparation, characteristics and reinforcing potential. *Carbohydr. Polym.* **2011**, *86* (3), 1198−1206.

(16) Mazega, A.; Signori-Iamin, G.; Aguado, R. J.; Tarrés, Q.; Ramos, L. P.; Delgado-Aguilar, M. Enzymatic pretreatment for cellulose nanofiber production: Understanding morphological changes and predicting reducing sugar concentration. *Int. J. Biol. Macromol.* **2023**, *253*, 127054.

(17) Henriksson, M.; Berglund, L. A.; Isaksson, P.; Lindström, T.; Nishino, T. Cellulose nanopaper structures of high toughness. *Biomacromolecules* **2008**, *9* (6), 1579−1585.

(18) Segal, L.; Creely, J. J.; Martin Jr, A.; Conrad, C. An empirical method for estimating the degree of crystallinity of native cellulose using the X-ray diffractometer. *Text. Res. J.* **1959**, *29* (10), 786−794.

(19) Gemo, C. M. *Determination of the ultimate aerobic biodegradability of plastic materials in an aqueous medium-method by analysis of evolved carbon dioxide*. ISO, 1999.

(20) Syverud, K.; Chinga-Carrasco, G.; Toledo, J.; Toledo, P. G. A comparative study of Eucalyptus and Pinus radiata pulp fibres as raw materials for production of cellulose nanofibrils. *Carbohydr. Polym.* **2011**, *84* (3), 1033−1038.

(21) Borrega, M.; Sixta, H. Purification of cellulosic pulp by hot water extraction. *Cellulose* **2013**, *20*, 2803−2812.

(22) Borrega, M.; Concha-Carrasco, S.; Pranovich, A.; Sixta, H. Hot water treatment of hardwood kraft pulp produces high-purity cellulose and polymeric xylan. *Cellulose* **2017**, *24*, 5133−5145.

(23) Sun, D.; Lv, Z.-W.; Rao, J.; Tian, R.; Sun, S.-N.; Peng, F. Effects of hydrothermal pretreatment on the dissolution and structural evolution of hemicelluloses and lignin: A review. *Carbohydr. Polym.* **2022**, *281*, 119050.

(24) Testova, L.; Borrega, M.; Tolonen, L. K.; Penttilä, P. A.; Serimaa, R.; Larsson, P. T.; Sixta, H. Dissolving-grade birch pulps produced under various prehydrolysis intensities: quality, structure and applications. *Cellulose* **2014**, *21*, 2007−2021.

(25) Hassan, S. Z.; Vinjamur, M. Analysis of sensitivity of equilibrium constant to reaction conditions for esterification of fatty acids with alcohols. *Ind. Eng. Chem. Res.* **2013**, *52* (3), 1205−1215.

(26) Bobleter, O. Hydrothermal degradation of polymers derived from plants. *Prog. Polym. Sci.* **1994**, *19* (5), 797−841.

(27) Akiya, N.; Savage, P. E. Roles of water for chemical reactions in high-temperature water. *Chem. Rev.* **2002**, *102* (8), 2725−2750.

(28) Cantero, D. A.; Tapia, Á. S.; Bermejo, M. D.; Cocero, M. J. Pressure and temperature effect on cellulose hydrolysis in pressurized water. *Chem. Eng. J.* **2015**, *276*, 145−154.

(29) SriBala, G.; Vinu, R. Unified kinetic model for cellulose deconstruction via acid hydrolysis. *Ind. Eng. Chem. Res.* **2014**, *53* (21), 8714−8725.

(30) Foelkel, C. *Papermaking properties of Eucalyptus trees, woods, and pulp fibers*; Eucalyptus online book & newsletter, 2009; pp. 110.

(31) Wang, Q.; Zhao, X.; Zhu, J. Kinetics of strong acid hydrolysis of a bleached kraft pulp for producing cellulose nanocrystals (CNCs). *Ind. Eng. Chem. Res.* **2014**, *53* (27), 11007−11014.
(32) Gao, M.; Shang, Y.; Li, B.; Du, H. Sustainable preparation of cellulose nanocrystals: state of the art and perspectives. *Green Chem.* **2022**, *24* (24), 9346−9372.
(33) French, A. D. Idealized powder diffraction patterns for cellulose polymorphs. *Cellulose* **2014**, *21* (2), 885−896.
(34) D'Acierno, F.; Michal, C. A.; MacLachlan, M. J. Thermal stability of cellulose nanomaterials. *Chem. Rev.* **2023**, *123* (11), 7295−7325.
(35) Wu, Q.; Meng, Y.; Wang, S.; Li, Y.; Fu, S.; Ma, L.; Harper, D. Rheological behavior of cellulose nanocrystal suspension: Influence of concentration and aspect ratio. *J. Appl. Polym. Sci.*, 2014, *131*, 15, .
(36) *ISO 14851:2019 Determination of the Ultimate Aerobic Biodegradability of PlasticMaterials in an Aqueous Medium_Method by Measuring the Oxygen Demand in a Closed Respirometer*, 2019. https://www.iso.org/standard/70026.html.
(37) Komiyama, K.; Omura, T.; Iwata, T. Effect of morphology and molecular orientation on environmental water biodegradability of poly [(R)-3-hydroxybutyrate-co-(R)-3-hydroxyvalerate]. *Polym. Degrad. Stab.* **2021**, *193*, 109719.
(38) Kumagai, S.; Hayashi, S.; Katsuragi, A.; Imada, M.; Sato, K.; Abe, H.; Asakura, N.; Takenaka, Y. One-Pot Synthesis of Marine-Biodegradable Poly (Ethylene Succinate)-Based Ester Amide Copolymers Containing Amino Acid. *ACS Appl. Polym. Mater.* **2024**, *6* (14), 8339−8347.
(39) Kümmerer, K.; Menz, J.; Schubert, T.; Thielemans, W. Biodegradability of organic nanoparticles in the aqueous environment. *Chemosphere* **2011**, *82* (10), 1387−1392.
(40) Miyaji, K.; Zhou, C.; Maeda, A.; Kobayashi, K.; Kusumi, R.; Wada, M. Biodegradation of various forms of cellulose and chitin in natural waters with different salinity. *Polym. Degrad. Stab.* **2023**, *215*, 110423.
(41) Boufi, S.; Kaddami, H.; Dufresne, A. Mechanical performance and transparency of nanocellulose reinforced polymer nanocomposites. *Macromol. Mater. Eng.* **2014**, *299* (5), 560−568.
(42) Rusli, R.; Eichhorn, S. J. Determination of the stiffness of cellulose nanowhiskers and the fiber-matrix interface in a nanocomposite using Raman spectroscopy. *Appl. Phys. Lett.* **2008**, *93* (3), 033111.

https://doi.org/10.1021/acs.biomac.4c01737
Biomacromolecules 2025, 26, 1372−1385